Catena 221 (2023) 106748

Contents lists available at ScienceDirect

Catena

journal homepage: www.elsevier.com/locate/catena

Changes in soil infiltration and water flow paths: Insights from subtropical forest succession sequence

Wanjun Zhang [a,b], Xiai Zhu [c], Xin Xiong [a,b], Ting Wu [a,b], Shuyidan Zhou [a,b], Zhiyang Lie [a,b], Xiaojin Jiang [c], Juxiu Liu [a,b,*]

[a] *Key Laboratory of Vegetation Restoration and Management of Degraded Ecosystems, South China Botanical Garden, Chinese Academy of Sciences, Guangzhou, 510650, China*
[b] *Guangdong Provincial Key Laboratory of Applied Botany, South China Botanical Garden, Chinese Academy of Sciences, Guangzhou, 510650, China*
[c] *CAS Key Laboratory of Tropical Forest Ecology, Xishuangbanna Tropical Botanical Garden, Chinese Academy of Sciences, Menglun, Yunnan, 666303, China*

A R T I C L E I N F O

Keywords:
Infiltrability
Soil water flow
Soil-rock interface
Root systems
Forest succession

A B S T R A C T

Maintaining and improving the water conservation capacity of forest ecosystems is an important step in building regional ecological protection barrier. At present, there is a lack of knowledge about the patterns of soil water flow in different stages of forest succession. Therefore, this study quantified the change tendency of soil infiltration and water flow paths in subtropical different forest types, including pine forests (PF), mixed pine and broadleaf forests (MF) and monsoon evergreen broadleaf forests (BF), and analysed the effect of soil physical properties on hydraulic properties. Results showed that (1) both BF and MF were characterized by a smaller bulk density and the larger porosity than PF. (2) The saturated hydraulic conductivity of BF and MF was 2.1 times and 3.1 times higher than that of PF, respectively, showing that there were clear differences in the soil infiltrability resistance of the different forest types. The observed soil water exchange amount also showed that both BF and MF had higher water holding capacity than PF. (3) Macropore flow and lateral flow were the dominant preferential flow behaviors, but the degree of preferential flow did not evolve along succession sequence PF, MF and BF. The pattern of soil water flow was found to show obvious spatial variability, restricted by the joint influence of soil porosity, root systems and rocks. The above results suggest that soil infiltration improve with the sequence of forest succession, but that soil water flow patterns may be independent of forest succession due to the complex conditions of the soil. This study provided effective data information of forest soil hydrological antecedents.

1. Introduction

Forest ecosystems play an important role in the process of hydrological cycle. Maintaining and improving forest water conservation capacity and water purification capacity has been a hot spot for a long time (Hua et al., 2022; Li et al., 2017). Soil layer is the vital hydrologic functional layer in the ecosystem, and soil water flow behavior is the key ‘conveyor belt’ to maintain the operation of various processes, connecting groundwater recharge, solution migration and plant water uptake (Zhao and Wang, 2021; Fuhrmann et al., 2019). The alternations in vegetation types, root systems, soil structures and properties change with the process of forest succession, which could affect soil water flow process (Zhu et al., 2019; Wang et al., 2012; Zhao et al., 2010). However, the mechanism of soil water flow in different forest succession stages is not clearly known yet. Therefore, it is needed to study of soil water flow mechanism in different succession stages, which would provide policy basis for forest water resources management and degraded-vegetation restoration (Surda et al., 2015).

Researchers have always reported an increasing need to have more knowledge on the interaction between land use, soil properties and soil hydrological processes (Di Prima et al., 2018; Bisantino et al., 2015; Bens et al., 2007). Generally, the water flow patterns of vadose zone affect the regional water exchange rate, because soil infiltration capacity and flow paths can lead to a redistribution of surface and groundwater. Soil water flow forms include matrix flow and preferential flow. Matrix flow is a relatively slow and even movement of water and solutes through soil while passing through all pore spaces (Allaire et al., 2009). Studies have shown that 70 %–85 % of soil water is related to preferential flow behavior (Hlaváčiková et al., 2019; Alaoui and Helbling, 2006). Preferential flow is a fast flow form of soil water and solute

* Corresponding author at: No. 723, Xingke Road, Tianhe District, Guangzhou, China.
E-mail address: ljxiu@scbg.ac.cn (J. Liu).

https://doi.org/10.1016/j.catena.2022.106748
Received 25 August 2022; Received in revised form 25 October 2022; Accepted 28 October 2022
Available online 15 November 2022

transport passing macropore channels, and it can accelerate water exchange (Beven and Germann, 1982). Zhu et al. (2019) demonstrated that the area with poor infiltrability is generally the source of surface runoff, while the area with good infiltrability and preferential flow development is the gathering area of water flow. For example, surface water can quickly infiltrate into the deep soil and meanwhile flows to the adjacent area in lateral direction. In soil layer, plant root can improve soil properties (e.g., soil pores) and facilitate water infiltration through the living roots embedding, entangling and enwrapping in soil (Niemeyer et al., 2014; Ludwig et al., 2005). In general, the macroporosity near the root zones is significantly greater than those in the non-root zone (Yue et al., 2021). In addition, the crack channels formed by stones can also support deeper water infiltration, accelerating the preferential flow process, and further promoting rapid solute transport (Wine et al., 2012; Jørgensen et al., 2002).

Some studies suggest that attention needs to be paid to the forest-water relationships in order to enhance water availability and increase resilience to climate-driven disturbances (e.g., drought and storm) (Song et al., 2022; Di Prima et al., 2017; Bisantino et al., 2015). Forest ecosystems change the spatio-temporal patterns of rainfall distribution through complex functional structures such as canopy, litterfall and soil layer (Yu et al., 2018; Crockford and Richardson, 2000). Accordingly, the increment or decrement of water volume and water flow form would show some differences in different forest ecosystems (Kuchment, 2022; Kurzweil et al., 2021). For example, it has been proposed that in the process of forest succession, vegetation types changing from grassland (primary community) to shrub and climax forest community, soil bulk density reduced and soil porosity increased significantly, thereby promoting water infiltrability (Zhao et al., 2010). But soil water storage decreased along with the natural vegetation succession due to the greater transpiration ability of trees than grasses (Zhang et al., 2016b). Subtropical forest is the ecological protection barrier in South China. At present, the forest water resources in this region are facing severe challenges due to the intense human activities (Zhao et al., 2019). The characteristics of soil water along forest successional gradient have been preliminarily acknowledged in this region, which help to recognize forest water conservation function (Liu et al., 2020; Yan et al., 2007). However, the knowledge of soil water flow patterns in different forest succession processes is not clearly known yet.

Therefore, in this study, we mainly focused on soil hydraulic properties and driving factors in different forest succession periods. Specifically, the objectives are to: (1) quantify the change tendency of soil infiltration and water flow paths along different succession forest types; (2) analyze the driving factors of soil infiltration and water flow paths in order to provide suggestions for forest water resources management. We hypothesized that: (1) soil infiltrability and preferential flow degree increased with forest succession sequences; (2) soil porosity, root systems and rocks jointly affect soil water flow patterns.

2. Materials and methods

2.1. Study area

This study was conducted at the Dinghushan Biosphere Reserve (23°09′21″N to 23°11′30″N, 112°30′39″E to 112°33′41″E) located in Zhaoqing City, south China. In Dinghushan, the catchment, consisting of two streams both with 12 km length, flow into the West River (the main trunk of the Pearl River). According to the Köppen-Geiger climate classification (e.g., Kottek et al., 2006), the study area belongs to tropical monsoon climate (Cwa) with obvious wet (April–September) and dry season (rest 6 months). The average annual temperature is 20.9 °C, and the annual rainfall and evaporation are 1900 mm and 1115 mm, respectively. According to the soil classification system of United States Department of Agriculture (USDA) (Buol et al. 2003), soils of Dinghushan area are classified in the Ultisol group and Udult subgroup, formed on the thick metamorphic sandstone and sand shale of Devonian period. The zonal soil was classified in the silt loam texture according to Word Reference Base (WRB) (WRB, 2015). Dinghushan Biosphere Reserve is covered with a complete horizontal succession series of monsoon evergreen broadleaf forest, which is highly representative of the region (Zhou et al., 2011). Monsoon evergreen broadleaf forest (BF) is 400 years old with typical tree species including *Castanopsis chinensis (Spreng.) Hance*, *Schima superba Gardner & Champ.*, *Cryptocarya concinna Hance*, etc., canopy coverage > 95 %. The slope is about 30°, and the elevation is about 270–300 m. Based on WRB, the soil was classified in texture of silt loam (sand 15–30 %, silt 50–60 % and clay 15–20 %), thickness of 60–90 cm, topsoil organic matter of 2.73–5.95 %. The mixed pine/broadleaf forest (MF) is a natural succession with a coniferous broadleaf ratio of about 4:6, 70–80 years old. The main broadleaf tree species are *Schima superba Gardner & Champ.*, *Castanopsis chinensis (Spreng.) Hance*, etc., and the coniferous specie is *Pinus massoniana Lamb*, canopy coverage > 90 %. The slope is about 30°, and the elevation is about 250 m. The soil type in MF was classified in texture of silt loam (sand 10–20 %, silt 60–70 % and clay 18–20 %), relatively shallow soil layer, topsoil organic matter of 2.94–4.27 %. The pine forest (PF) planted before 1960 belongs to the primary succession community where *Pinus massoniana Lamb* is the only tree layer with the canopy coverage of about 70 %. The slope is about 25°–30°, and the elevation is about 250–300 m. The soil was classified in texture of loam above 40 cm (sand 30–40 %, silt 40–50 % and clay 10–15 %) and silt loam below 40 cm (sand 25–30 %, silt 50–60 % and clay 15–20 %), relatively shallow soil layer, topsoil organic matter of 1.33–2.97 %.

2.2. Basic data of soil properties

Experiments in this study were conducted in three forest types (BF, MF and PF) between November and December in 2021 (Fig. 1). Sampling plots were selected following the similar slope and direction in each of the three forest types. Bulk soil samples were collected to measure soil bulk density (g cm^{-3}) and porosity (%) at each of five depths 0–10, 10–20, 20–40, 40–60 and 60–100 cm using cutting cylinders (volume, 100.0 cm^{3}) in 2005, 2010, 2015 and 2020, respectively. The mean value of the four-year data (2005, 2010, 2015 and 2020) was calculated, shown in the Table 1. Data of soil water content and water potential were monitored at above five depths using sensors (Hydra Probe II, USA; Tensio 100, Germany) in 2020, which was used to fitted soil water characteristic curves (SWCC) of different depths based on Gardner model (Gardner et al., 1970). In addition, in order to estimate the response of soil moisture to rainfall events, soil water content (SWC) at soil depths 10 cm, 30 cm and 50 cm was monitored using TDR (Hydra Probe II, USA) (Fig. 1). Tipping-bucket rain gauge were installed 400 m away from the TDR plots, and rainfall data were recorded using a data logger (Model 115, Spectrum Technologies Inc., USA). The resolution of the rain gauge was ± 0.2 mm, and the time interval of data recording was set to 10 min.

2.3. Infiltration measurement

The soil saturated hydraulic conductivity was measured at the soil surface using the stainless-steel double rings (height, 20.0 cm; outer ring diameter, 50.0 cm; inner ring diameter, 25.0 cm), 8 repetitions in each forest land. Double rings were both embedded into the soil depth 10.0 cm, exposing to a height of 10.0 cm. Double rings were both initially filled with water equivalent to a water head of 10.0 cm, and the reduced water level height of inner ring was recorded at 2-min intervals for the first 10 min and then 5-min intervals for at least 50 min. The initial infiltration rate (*IIR*, cm min^{-1}) was defined as the ratio of the reduced water depth to the initial infiltration time (2 min). Each cylinder was rapidly refilled to a height of 10.0 cm after each recording until the difference in water level between filling and after 5 min remained the same for five consecutive times. The water refilling procedure of infiltration took approximately 1.0 h. We assumed that a steady-state flow

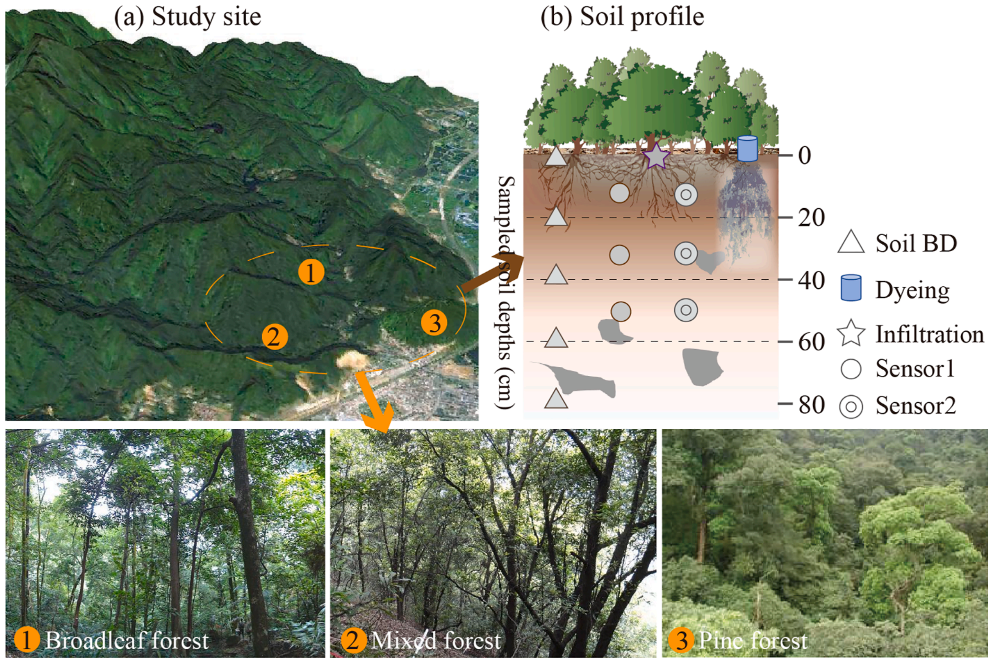

Fig. 1. (a) Study site within the Dinghushan Biosphere Reserve in China and (b) sampling from the soil profile in three forest types. Soil BD, soil bulk density. Sensor1 was used to monitor soil water content; Sensor2 was used to monitor soil water potential.

occurred at this point, and the actual steady state infiltration rate (*Is*, cm min^{-1}) was calculated based on the last five measured values (Bodhinayake et al., 2004). Due to water temperature affecting *Is*, the *Is* was converted to the quasi-steady infiltrate rate (*SIR*, cm min^{-1}) at 10 °C, and the *SIR* was used to calculate the soil saturated hydraulic conductivity (*Ks*, cm min^{-1}) (Reynolds and Elrick, 1990):

$$\mathrm{SIR} = \frac{\mathrm{I_s}}{0.7 + 0.03\mathrm{T}} \tag{1}$$

$$\mathrm{Ks} = \frac{\mathrm{SIR}}{\frac{\mathrm{H_s}}{\mathrm{C_1 d_s + C_2 r_s}} + \frac{1}{\mathrm{S(C_1 d_s + C_2 r_s)}} + 1} \tag{2}$$

where $T = 20$ °C indicates the actual water temperature of *Is* state; $C_1 = 0.316\pi$ and $C_2 = 0.184\pi$ are dimensionless constants. H_s is the height (10 cm) of water inside the cylinder, d_s is the rest of height (10 cm) of cylinder, r_s is the radius of the cylinder, and *S* is the sorptive number (12 cm^{-1}).

After the infiltration experiment, the infiltration rings were taken away, then litter were collected into valve bag, oven-dried at 85 °C for 24 h to calculate litter biomass. The soil surface was cut flat, and soil samples were collected using cutting ring at each of the infiltration point, and the bulk density and porosity are measured. Further, the influence of soil physical properties on the infiltration rate was analyzed.

2.4. Dye-tracer experiment

Brilliant Blue FCF dye was used to trace soil water flow paths in the three forest types, three repetition in each type with total 9 plots (B1 ~ B3, M1 ~ M3 and *P*1 ~ *P*3). Stainless-steel ring (height, 20.0 cm; diameter, 25.0 cm) was driven into the soil depth 10.0 cm, 90 L solution was prepared with dye concentration 4.0 g L^{-1}. 10 L solution was injected into those 9 plots, respectively. After 24 h, cut the soil dyeing profiles 70 cm width × 70 cm depth (Fig. 1). Soil profile was photographed and recorded. Combined with the corresponding scale of the image processing software and the field profile, the image of the dyed profile was corrected.

The dyeing images were processed using Software ArcMap 10.3 (ESRI Inc., Redlands, California, USA). Firstly, the dyeing areas were classified into three kinds of concentrations by the supervised classification: dark (heavy stain), moderate (moderate stain) and light (low stain) dyeing area. The dark area indicates the active macropore flow area; the light area indicates the interactions between the macropore flow and the surrounding matrix flow, respectively (Jiang et al., 2015). In addition, preferential flow indices were calculated using 20 cm width × 20 cm depth image, separated from the 70 cm width × 70 cm depth image. Preferential flow indices included the dyeing coverage rate (*DC*, %), uniform infiltration depth (*UID*, cm), preferential flow fraction (*Pf-fr*, %), length index (*LI*) and peak index (*PI*), respectively (Bargués Tobella et al., 2014; van Schaik, 2009; Flury et al., 1994).

$$DC = \frac{S_{dye}}{S} \times 100\% \tag{3}$$

where S_{dye} is the dye-stained area (cm^2), and *S* is the total profile area (cm^2), dye-stained area plus non-strained area;

$$Pf - fr = \left(1 - \frac{UID \times W}{S}\right) \times 100\% \tag{4}$$

where *UID* is the depth at which the *DC* decreases below 80 %, indicating the depth to which matrix flow is prevalent; *W* is the soil profile width 20 cm.

$$\mathrm{LI} = \sum_{i=1}^{70} |DC_{i+1} - DC_i| \tag{5}$$

where *i* is the depth interval of the rectangular area in which dye coverage (*DC*, %) was calculated. A high *LI* indicates a high degree of preferential flow.

PI is the number of times that the vertical line defined by the dye coverage (*DC*) intersects the dye coverage profile. High value of *PI* indicates a high degree of preferential flow.

2.5. Other relevant measurements

After photographing and recording, each dyeing soil profile was divided into 10 × 10 cm square grids. Roots and bulk soil samples in the grids were collected in order to evaluate the relationships between grid dyeing area and root biomass and soil physical properties. A total of 30

Table 1
Soil physical properties and hydrological properties at 0–100 cm depths in three forest types. BF: broadleaf forest, MF: mixed pine/broadleaf forest, PF: pine forest. BD, bulk density; TP, total porosity; FWC, field water capacity; SaWC, saturated water capacity. SWCC, soil water characteristic curve. The different lowercase letters a, b and c indicate significant differences between the slopes ($P < 0.05$). Letter 'θ' indicates soil volumetric water content. Letter 'S' indicates soil suction. Letter 'A' presents the water holding capacity, the higher A value, the stronger water holding capacity. Letter 'B' presents the decrease rate of soil water content with the increase of soil water suction, the larger B value, the faster change.

Soil depths	Plots	BD (g cm^{-3})	TP (%)	FWC (%)	SaWC	SWCC ($\theta = A \times S^{-B}$)
0–10 cm	BF	1.10 (0.04) b	53.72 (1.10) a	33.21 (1.27) a	55.82 (3.80) a	$\theta = 29.397 \times S^{-0.144}$, $r^2 = 0.970$
	MF	1.15 (0.07) b	52.82 (0.95) a	30.24 (2.48) a	50.92 (1.40) a	$\theta = 27.932 \times S^{-0.131}$, $r^2 = 0.961$
	PF	1.43 (0.09) a	41.87 (0.65) b	21.59 (2.02) b	42.77 (2.41) b	$\theta = 16.056 \times S^{-0.185}$, $r^2 = 0.978$
10–20 cm	BF	1.28 (0.05) b	50.13 (0.43) a	30.69 (0.24) a	52.83 (2.66) a	$\theta = 28.576 \times S^{-0.111}$, $r^2 = 0.964$
	MF	1.29 (0.09) b	49.95 (1.17) a	28.37 (1.07) a	48.84 (0.78) a	$\theta = 26.116 \times S^{-0.131}$, $r^2 = 0.963$
	PF	1.51 (0.02) a	40.53 (0.75) b	21.98 (2.52) b	39.86 (1.41) b	$\theta = 14.763 \times S^{-0.179}$, $r^2 = 0.974$
20–40 cm	BF	1.32 (0.09) a	48.20 (0.56) a	27.87 (1.08) a	48.42 (1.15) a	$\theta = 25.370 \times S^{-0.119}$, $r^2 = 0.966$
	MF	1.30 (0.12) a	45.73 (0.70) a	28.00 (1.44) a	44.71 (2.97) a	$\theta = 22.875 \times S^{-0.135}$, $r^2 = 0.958$
	PF	1.53 (0.09) a	39.85 (0.65) b	19.34 (1.09) b	39.03 (0.23) b	$\theta = 15.203 \times S^{-0.165}$, $r^2 = 0.975$
40–60 cm	BF	1.41 (0.04) a	48.73 (0.95) a	26.07 (1.34) a	45.14 (0.42) a	$\theta = 22.444 \times S^{-0.135}$, $r^2 = 0.958$
	MF	1.42 (0.03) a	43.86 (0.49) b	24.55 (0.14) b	42.83 (1.65) b	$\theta = 21.586 \times S^{-0.111}$, $r^2 = 0.971$
	PF	1.52 (0.08) a	39.13 (0.78) b	20.59 (0.54) b	40.03 (0.37) b	$\theta = 17.111 \times S^{-0.143}$, $r^2 = 0.976$
60–100 cm	BF	1.31 (0.23) a	47.55 (0.87) a	26.66 (0.55) a	42.86 (2.61) a	$\theta = 23.133 \times S^{-0.128}$, $r^2 = 0.958$
	MF	1.47 (0.08) a	41.40 (0.82) b	24.82 (0.34) b	37.93 (2.64) b	$\theta = 21.943 \times S^{-0.111}$, $r^2 = 0.956$
	PF	1.43 (0.08) a	38.51 (0.70) b	21.09 (0.33) b	39.53 (0.22) b	$\theta = 17.977 \times S^{-0.144}$, $r^2 = 0.958$
Summary of ANOVA (*P* value)						
Plot		< 0.001	< 0.001	< 0.001	< 0.001	–
Depth		< 0.001	< 0.001	< 0.001	< 0.05	–
Plot × Depth		0.119	0.218	0.4	0.38	–

Notes: mean (±SE), $n = 4$.

root samples were picked and brought back to the laboratory. Root surface was washed and water was removed from the surface with absorbent paper. Roots were classified in two groups based on the diameter: thick (>2 mm); and fine (<2 mm). After oven-dried at 85 °C for 24 h to constant weight, roots were weighed for obtaining root biomass (±0.01 g). A total of 35 bulk soil samples were taken to the laboratory for determining soil bulk density, porosity and water capacity.

2.6. Data analysis

One-ANOVA was used to estimate the differences in soil bulk density, porosity, infiltration rate and saturated hydraulic conductivity among different forest types. Differences of soil properties among soil depths and sampling plots were analysed using general linear models with 'depth' and 'plot' as fixed effects. Pearson correlation analysis was performed to evaluate the effect of soil physical properties on hydraulic properties. All data processing and analysis were performed at $\alpha = 0.5$ with IBM SPSS Statistics 25. Graph was drawn in Origin 9.0.

3. Results

3.1. Soil physical properties

In succession sequence, change of forest soil physical properties was significant from early, middle to climax communities. The average values of four-year data (2005, 2010, 2015 and 2020) were shown in Table 1. In detail, the soil bulk density of pine forest (1.42 g cm^{-3}) was significantly higher than that of mixed forest (1.12 g cm^{-3}) and broadleaf forest (1.18 g cm^{-3}) (Table 1). Compared with pine forest, soil total porosity in mixed forest and broadleaf forest increased by 26.15 % and 28.3 %, respectively. Soil bulk density increased and total porosity decreased with the increasing soil depths. Analysis of variance (ANOVA) showed that soil bulk density and porosity were significantly different at different soil depths ($P < 0.001$).

The measurement of soil field water capacity showed significantly decreasing tendency BF (28.90 %) > MF (27.20 %) > PF (20.92 %), and from topsoil (30.23 %) to 100 cm depth (24.82 %). Similar decreasing tendency was also presented in the soil saturated water capacity. In addition, soil water characteristic curve can also be used to characterize soil hydraulic characteristics, the fitted model result was the same tendency with the observation, showing that soil water holding capacity ('A' value) of broadleaf forest was stronger (29.397) than that of mixed forest (27.932) and pine forest (16.056) (Table 1). Soil water holding capacity of broadleaf forest and mixed forest decreased with the increasing soil depth, while that of pine forest increased slightly with the increase of soil layer.

3.2. Soil water infiltration rate

Soil water infiltration rate of the three forest types all showed a trend of decrease over time, with a sharply decrease in the first 10 min and then gradually decrease until steady state (Fig. 2). The initial infiltration rate of broadleaf forest and mixed forest was 2.1 times and 2.9 times of pine forest, respectively. The saturated hydraulic conductivity of broadleaf forest and mixed forest was 2.1 times and 3.1 times of pine forest, respectively. Therefore, the soil infiltration capacity of broadleaf forest and mixed forest was significantly higher than that of pine forest ($P < 0.05$).

Soil moisture timely responded to rainfall events and was obviously supplied. After reaching the wetting front, soil moisture gradually subsided (Fig. 3). The results of one-month soil moisture continuous monitoring showed that the surface SWC fluctuated greatly, while the sublayer SWC fluctuated little ($CV_{surface} > CV_{sublayer}$). Among different forest types, both the fluctuation degrees of SWC in the broadleaf forest and the mixed forest were smaller than that in the pine forest (CV_{BF} & $CV_{MF} < CV_{PF}$). For the two recorded rainfall events (22.8 mm and 30.2 mm), larger supplement amount (↑10.0 %) of soil water was found in the broadleaf forest, and smaller depletion amount (↓0.2 %) of soil water was found in the mixed forest. In addition, for water exchange of different soil depths, both soil water supplement amount and depletion amount of broadleaf forest and mixed forest were greater in the surface

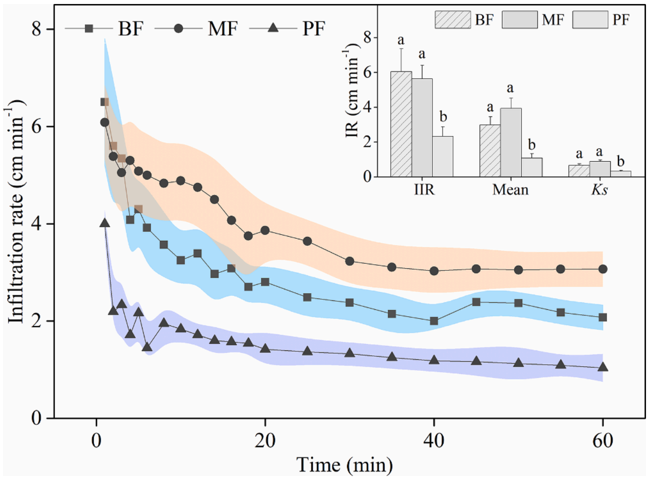

Fig. 2. Variation of infiltration rate with time, and initial infiltration rate (IIR, cm min^{-1}), mean infiltration rate (Mean, cm min^{-1}), and saturated hydraulic conductivity (*Ks*, cm min^{-1}) for three forest types. BF: broadleaf forest, MF: mixed pine/broadleaf forest, PF: pine forest. Data are expressed as the mean ± standard error (n = 21). Different letters indicate a significant difference at $P < 0.05$.

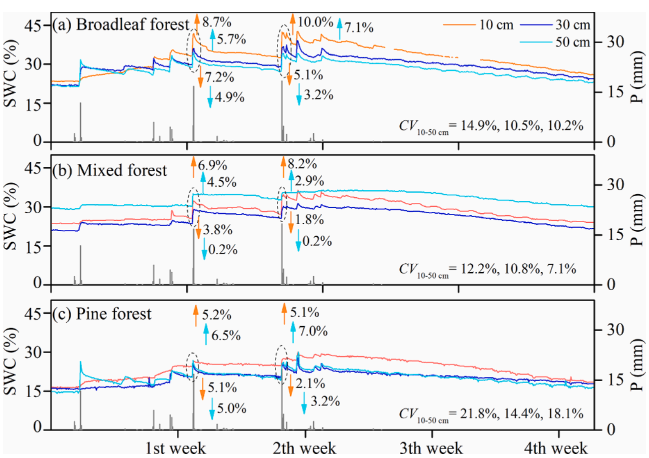

Fig. 3. Change of soil water content (SWC) at different soil depths in response to rainfall events. Orange arrow means 10 cm depth and cyan arrow means 50 cm depth. The upward arrow represents supplement amount and the downward arrow represents depletion amount. (For interpretation of the references to colour in this figure legend, the reader is referred to the web version of this article.)

layer (10 cm) than that in the deeper layer (50 cm), while both the increment and the decrement of soil water of pine forest were lower in the surface layer (↑5.1 %, ↓2.1 %) than that in the deeper layer (↑7.0 %, ↓3.2 %) indicating higher soil water exchange degree in the deeper layer.

3.3. Soil water flow paths

After injecting the same dye solution volume to the 9 plots, the infiltration depth mainly was at 60–70 cm, even above 70 cm in the B2, M2 and M3 (Fig. 4). Proportions of the stained soil areas showed the spatial variability of soil water flow at the different soil depths in the three forest types. In the broadleaf forest (B1–B3), mean dye coverage was 41.63 % ± 3.76 % (n = 3), of which high stained area was 20.56 %. Dye coverage of high stained area in the B2 plot had two peak point at depth 5 cm and depth 60 cm, respectively, different from the other two plots. In the mixed forest (M1–M3), mean dye coverage was 44.79 % ±2.16 % (n = 3), of which high stained area was 16.85 %. The maximum dye coverage was 88.04 %, appearing at depth 30 cm of M1 plot, indicating that lateral permeation was obvious. The high stained area of M1–M3 plots mainly distributed above depth 30 cm, and the moderate and low stained area is mainly below. In the pine forest (*P*1–*P*3), mean dye coverage was 32.57 %±6.23 % (n = 3), of which high stained area was 14.82 %. The dye coverage of high stained area decreased with soil depth in the *P*1 and *P*3 plots. Differently, it first increased above depth 30 cm in the *P*2 plot, and then decreased.

Preferential flow indices and stained soil profiles (20 cm width × 20 cm depth selected) were shown in Fig. 5. Infiltration depths (*ID*) varied among different plots, the maximum *ID* in broadleaf forest (>70 cm) and mixed forest (>70 cm) were deeper than that in pine forest (67 cm). Uniform infiltration depth (*UID*) of the pine forest appeared at shallower depth (16.0 cm) than those of the broadleaf forest (31.0 cm) and the mixed forest (24.0 cm). Dye coverage (*DC*) of the broadleaf forest (78.2 % ± 2.3 %) and the pine forest (74.8 %±5.3 %) were greater than that of the mixed forest (66.1 %±4.1 %). By comparison, preferential flow fraction (*Pf-fr*) of the pine forest (46.8 %±5.3 %) was greater than those of the broadleaf forest (23.2 %±10.0 %) and the mixed forest (30.0 ± 10.4 %). Both length index (*LI*) and peak index (*PI*) of the mixed forest averagely were higher than those of the broadleaf forest and the pine forest. Comparing the preferential flow indices among the three forest types, high spatial variability of soil water flow was found, and the preferential flow degrees varied with different sampling plots without along forest succession sequence.

3.4. Correlation between water and soil variables

Soil bulk density and porosity are soil basic physical properties. A significantly negative relationship was found between bulk density and root biomass (r = 0.53, $P < 0.01$, n = 23), and significantly positive relationship between porosity and root biomass (r = 0.45, $P < 0.05$, n = 23) (Fig. 6). No significant relationship between root biomass and non-capillary porosity was found ($P > 0.05$).

Correlation analysis results showed that the initial infiltration rate was negatively correlated with initial water content (r = 0.43, $P < 0.05$, n = 23) and bulk density (r = -0.46, $P < 0.05$, n = 23), positively correlated with porosity (r = 0.46, $P < 0.05$, n = 23). The saturated water conductivity was significantly affected by bulk density (negative correlation) and porosity (positive correlation). No significant relationship was found between topsoil litter & root biomass and infiltration rate ($P > 0.05$).

Dyeing area were significantly correlated with bulk density, porosity and root biomass. And the strongest correlation was found between root biomass and dyeing area (r = 0.80, $P < 0.001$, n = 23). With the pore channel generated between root and soil, water flow was active and preferential flow degree was developed.

4. Discussion

4.1. Change of soil infiltration

In the present study, soil bulk density decreased and soil porosity tended to increase along the succession gradient of long-term natural vegetation, which contributed to increasing soil water conductivity and water-holding capacity and thereby promoting efficient infiltration volume of rainfall (He et al., 2019; Zhang et al., 2016b). Soil infiltration capacity in broadleaf forest and mixed forest both were stronger than that in pine forest (Fig. 2). The variation patterns (i.e., trend of increase or decrease) of soil properties (bulk density and porosity) and infiltration were consistent with the succession gradients. Besides, the litter layer of surface layer is effective at intercepting rainwater, and litter decomposition can improve soil properties (Zhu et al., 2021; Watanabe et al., 2013). According to previous statistics in Dinghushan area (Liu

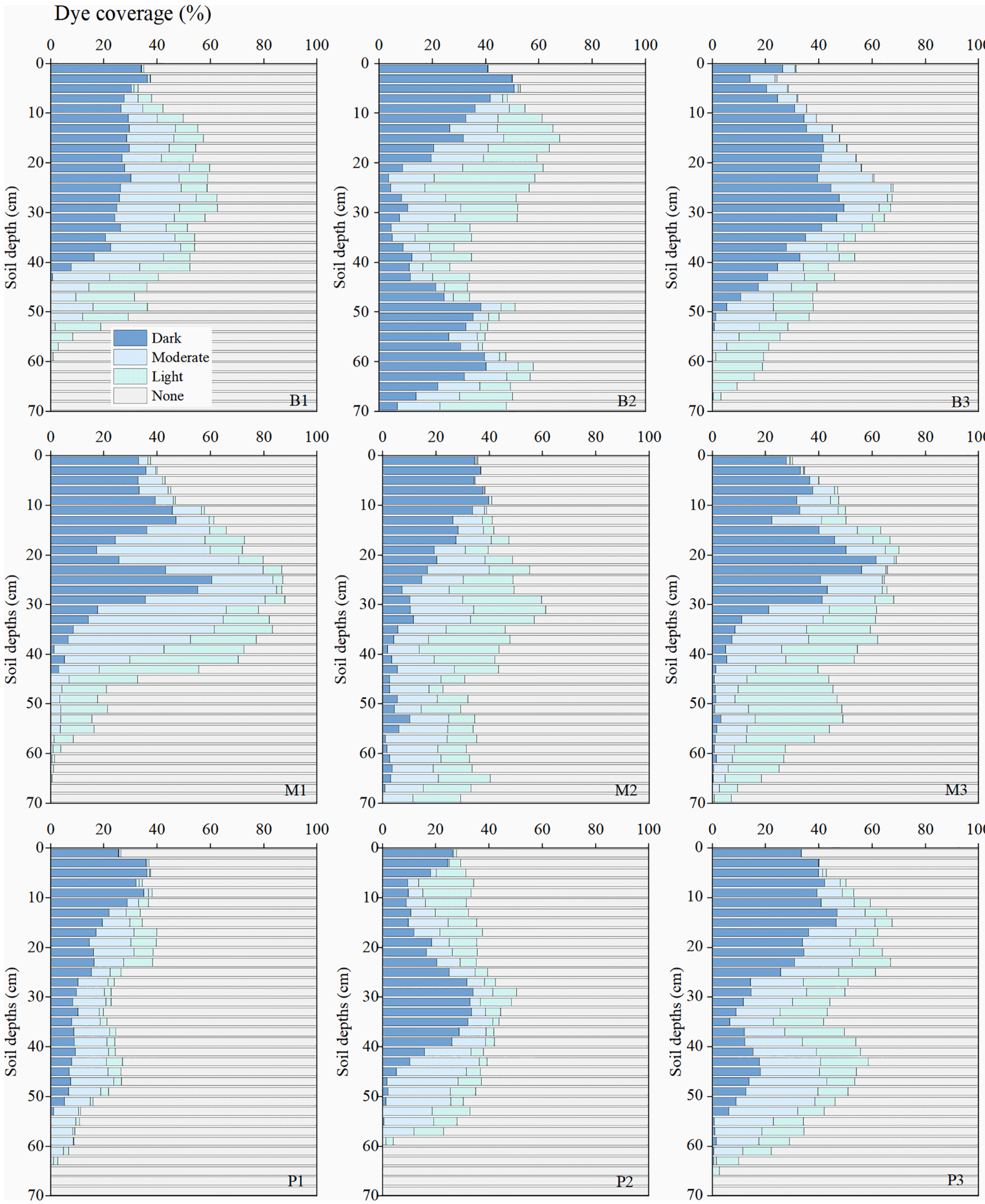

Fig. 4. Proportions of stained areas at different soil depths with 2 cm apart on the dyeing sections (depth 70 cm × width 70 cm) in the three forest types. B1 ~ B3 were in broadleaf forest, M1 ~ M3 were in the mixed forest, and *P*1 ~ *P*3 were in pine forest.

et al., 2013), the litter biomass along the forest successional gradient was in the order of PF > MF > BF, and PF litter had a higher water-holding ability than the other two forest types. Besides, litter from PF decomposes slowly due to its high lignin and low nitrogen content (Chae et al., 2019; Sheffer et al., 2015). Probably higher decomposition of BF and MF forest residues increase soil organic matter in surface horizons. Therefore, the indirect effect of litter on infiltration is positive due to the transformation of litter to organic matter is beneficial to the improvement of soil physical and chemical properties (Liu et al., 2021; Piaszczyk et al., 2020). However, this study showed no significant relationship between litter biomass and infiltration rate (Fig. 6). On the one hand, the poor cohesion among plant debris was conducive to the rapid passage of water flow through litter layer, causing invalid water interception (Neris et al., 2013); on the other hand, water injection volume in the infiltration experiment potentially covered the initial water interception of litter layer. More measurements would be needed to validate the finding for interaction between soil water flow and litter and soil organic matter.

When rainwater infiltrating into soil layer, some difference in the amount of soil water supplement/depletion among these three forest types were found. The monitoring results showed that soil water supplement amounts of both broadleaf forest and mixed forest were higher at surface layer than at deeper layer, while the opposite situation was observed in pine forest (Fig. 3). The soil porosity of broadleaf forest and mixed forest at surface layer was obviously higher than that at deeper layer, leading to faster water exchange and greater water volume variation. Soil bulk density and porosity in pine forest showed relatively small changes among four sampled layers 0–60 cm (Table 1), thus small

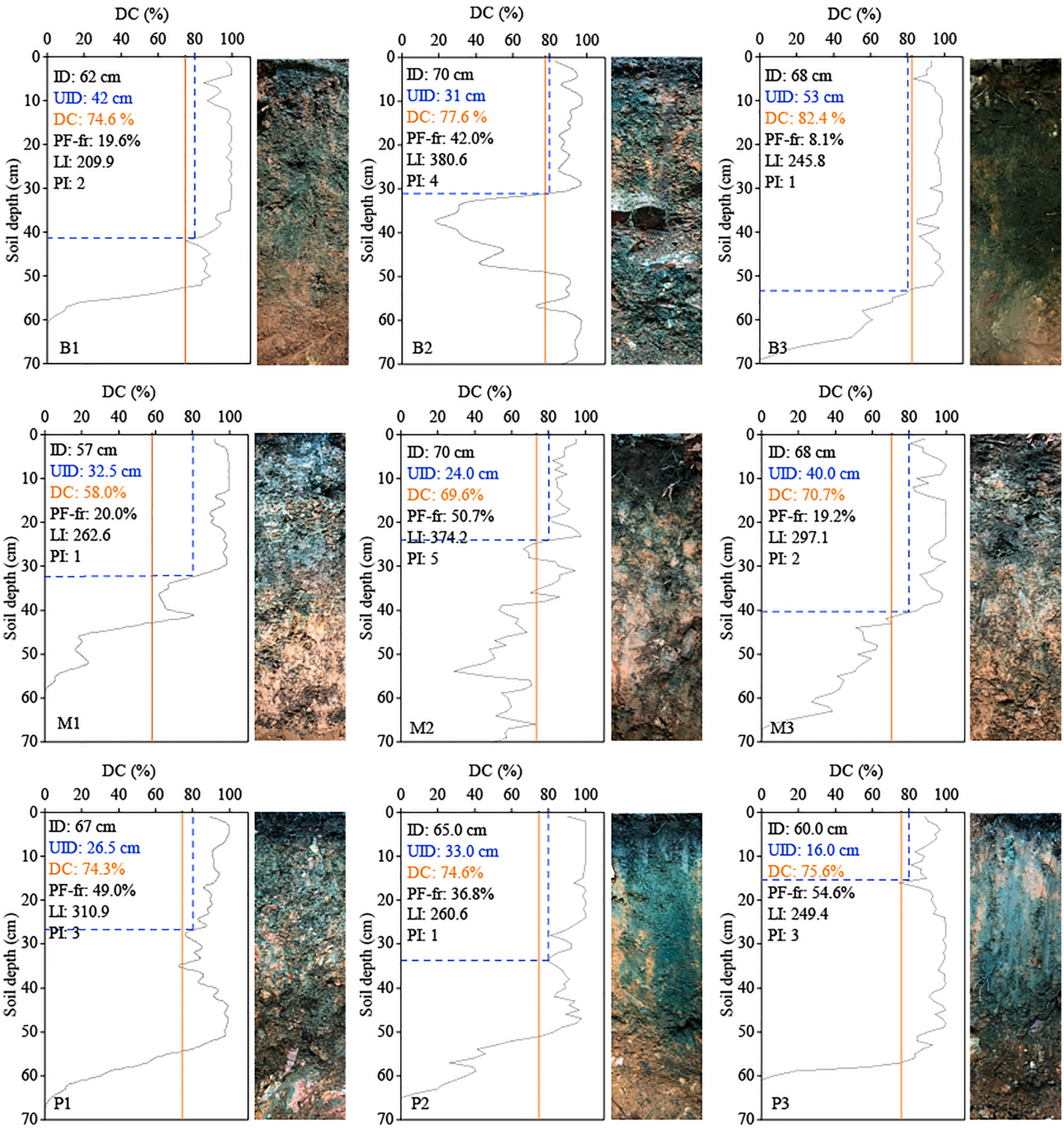

Fig. 5. Changing of dyeing coverage with soil depths at the dyeing profiles, depth 70 cm × 20 cm width for three forest types. B1 ~ B3 were in broadleaf forest, M1 ~ M3 were in the mixed forest, and *P*1 ~ *P*3 were in pine forest. The indices were used to evaluate the degree of preferential flow. ID: Infiltration depth (cm), UID: Uniform infiltration depth (cm), namely the intersection of the blue dotted lines and dye coverage (black lines), DC: Dye coverage (%) (orange line), Pf-fr: Preferential flow fraction (%), LI: Length index, PI: Peak index. (For interpretation of the references to colour in this figure legend, the reader is referred to the web version of this article.)

difference of rainfall supplement amount was found between 10 cm and 50 cm soil layers. Moreover, the depletion amount of mixed forest was relatively small compared with that of broadleaf forest and pine forest, thus the soil water-holding capacity in mixed forest was likely to be stronger than the other two forest types. In addition, due to the rapid evaporation of water and rich soil porosity in the surface soil, the intense water exchange here resulted in the larger water depletion amount in the surface soil than in the deep soil. This also indicated that the deeper soil was the key layer for water conservation. The soil moisture of both broadleaf forest and pine forest were higher at 10 cm depth than at 50 cm depth (Fig. 3). The soil water content of mixed forest was in the medium level at the 10 cm, and in the high level at the 50 cm. He et al. (2019) observed the same phenomenon in the soil moisture monitoring experiment in Qinghai Spruce (*Picea crassifolia*) forest, which was attributed to the interaction between water consumption and supplement. On the one hand, root systems were generally concentrated in the surface soil with great soil evapotranspiration and plant water consumption. On the other hand, soil moisture was partially replenished by rainfall infiltration. Consequently, great consumption and partial supplement made the surface soil water at a moderate level. The deeper soil generally has less root systems and lower plant water consumption as well as great supplement by rainfall infiltration during the rainy season, resulting in the maximum soil moisture in the deeper soil (Penna et al., 2013). Thus, increasing the water-holding capacity of the deeper soil can effectively alleviate the water demand of plants and reduce groundwater recharge during the dry season (Heathman et al., 2012).

	Lf	BD	TP	CP	NCP	RB	tRB	IWC	SWC	IIR	Ks	DA
BD	0.32											
TP	-0.32	–0.99										
CP	-0.32	–0.94	0.94									
NCP	-0.09	–0.77	0.77	0.69								
RB	N	–0.53	0.45	0.47	0.25							
tRB	N	–0.66	0.33	0.29	0.32	0.67						
IWC	-0.13	–0.87	0.87	0.88	0.65	N	N					
SWC	–0.27	–0.99	0.99	0.92	0.78	0.60	0.78	0.86				
IIR	–0.02	–0.46	0.46	0.50	0.73	N	N	0.43	0.46			
Ks	–0.03	–0.48	0.48	0.51	0.68	N	N	0.53	0.48	0.77		
DA	N	–0.50	0.51	0.42	0.49	0.51	0.45	N	0.50	N	N	
hDA	N	–0.59	0.37	0.28	0.42	0.80	0.75	N	0.63	N	N	0.63

Fig. 6. Relationships between soil physical properties and hydrological properties (n = 23). Soil physical properties refer to Lf, Litterfall mass; BD, bulk density; TP, total porosity; CP, capillary porosity; NCP, non-capillary porosity; RB, root biomass; tRB, thick root biomass. Soil hydrological properties refer to IIR, initial infiltration rate; Ks, saturated hydraulic conductivity; SWC, saturated water capacity; DA, dyeing area; hDA, high-concentrated-dyeing area. 'N' means no data. Grey area indicates no significance test, $P > 0.05$. Blue area indicates $P < 0.05$. Orange area indicates $P < 0.01$. Red area indicates $P < 0.001$. (For interpretation of the references to colour in this figure legend, the reader is referred to the web version of this article.)

Among the three forest types, the soil surface infiltrability of pine forest was lower than that of broadleaf forest and mixed forest, and the saturated accounted for 49.3 % and 37.4 % of broadleaf forest and mixed forest, respectively. Neris et al. (2013) also revealed that the soil infiltration rate of the pine forest was 60 % lower than that of the tropical rainforest, resulting in the twice higher surface runoff of the pine forest than that of the tropical rainforest. This result was partially attributed to the surface soil properties. A water drop penetration time method (WDPT) was used to measure soil water repellency (SWR) of topsoil of the three forest types in our study. The duration of water penetration was recorded, classifying repellency into four levels based on King (1981), none (<1 s), extremely slight (1–10 s), slight (10–60 s). Result showed that the time of broadleaf forest and mixed forest were < 1 s, none repellency, while pine forest was about 4 s, the extremely slight repellency (Table S1). Therefore, water repellency of pine forest was slightly higher than that of broadleaf forest and mixed forest. The lower soil infiltration rate in the pine forest was potentially caused by greater persistence of SWR. Although the soil infiltrability of pine forest was relatively weak, the part preferential flow activity was stronger than mixed forest, and thus the soil macropores of pine forest are potentially conductive to transport more water. According to the soil properties measured in our study site and the results found by Doerr et al. (2000), the reason could be that rocks, fissures and cracks in the water-repellent soil layer provided macropore channels for water flow. Soil infiltrability at the soil surface can directly affect runoff yield under rainstorm events. Therefore, more attention should be paid to erosion of pine forests in areas with sparse surface cover or bare soil. Meanwhile, in rocky areas, preferential flow may be more active and require more attention to the effects of chemical solute migration.

4.2. Change of soil water flow paths

Dyeing tracer technology well visualized some differences of soil water flow paths in different forest types. The spatial variability in water flow paths was potentially attributed to the spatial heterogeneity of soil conditions. In Dinghushan area, the soil in the broadleaf forest and mixed forest were found to have higher porosity and infiltrability than the pine forest (Table 1, Fig. 2), however, the degree of preferential flow within a width of 20 cm did not show the similar tendency according to the indices result. The quantitative indices (e.g., *ID*, *UID*, *DC*, *Pf-fr*, *LI* and *PI*) clearly showed the development degree of preferential flow in vertical direction (Fig. 5). By comparison, it was the pine forest that showed stronger preferential flow based on *UID* and *Pf-fr*, while the mixed forest showed stronger degree based on *LI* and *PI* or the broadleaf forest showed stronger degree based on *ID* and *DC*. The development degree of preferential flow of three forest types did not entirely evolve along the succession sequence PF → MF → BF, though the broadleaf forest has superior soil conditions, such as rich soil porosity produced by root activity and litter decomposition (Jiang et al., 2020). Similarly, Surda et al. (2015) also found the order of changes in soil water penetration depths was different from the succession gradients. However, such result within a width of 20 cm possibly ignored the presence of lateral flow activity. The result of the dye coverage within a width of 70 cm indicated that there is stronger lateral flow in the broadleaf forest and mixed forest than in the pine forest (Fig. 4). Combing with soil condition, infiltration rate and the indices, soil water potentially presented faster flow (lateral flow) in the broadleaf forest and mixed forest than in the pine forest.

From the perspective of soil structure of dyeing profile, some areas surrounded by considerable stones presented a large proportion of dye area with active water movement (Fig. 5). Stones in the soil was characterized by changing the path of soil water migration. In gravelly areas, e.g., *P*1 plot and *P*3 plot of the pine forests, gaps between rocks and soil provided preferential flow paths, thereby facilitating water infiltration (Hlaváčiková et al., 2019; Zhang et al., 2016a). Meanwhile, connectivity of soil pores was also considered to be the key for water transport (Jačka et al., 2021; Soracco et al., 2019). In the B2 plot of broadleaf forest (Fig. 5), the gap channels among rocks achieved good connectivity so as to promote water transport. Consequently, the dyeing concentration was high and dyeing area was large in the rock distribution area. However, no obvious rocks were found in the B1 plot of the broadleaf forest and the M1 plot of mixed forest soil profiles, and preferential flow was simply concentrated in shallow soil layer. In the non-rock region, soil macropores likely depended on the limited root distribution of systems and fauna activities. As a result, water infiltration was blocked, and the preferential flow phenomenon was weakened in the deep soil (Di Prima et al., 2018; Ameli et al., 2016). This was consistent with the results of Peng et al. (2022) and Sohrt et al. (2014), who revealed that surface runoff penetrated faster and deeper along the rock-soil interface, while the infiltration pattern of water in the soil was relatively more uniform. In addition, lateral flow was a kind of preferential flow form with water lateral migration and was considered as a potential water source of matrix flow (Jačka et al., 2021; Anderson et al., 2009). Because of the water infiltration obstruction vertically, a relatively wide stained area would appear, indicating the lateral flow phenomenon. At the depth of 30 cm in the soil dyeing profile of mixed forest M1 plot, > 90 % of the total area was stained (Fig. 4). On average, the degree of lateral flow in the pine forest was weaker (dye area < 70 %) than in the broadleaf forest and mixed forest. A study on the loess slopes found that large rock cover in soil layer contributed to the dominant lateral flow phenomenon and significantly affected the spatial distribution of water infiltration (Mei et al., 2018). In forest rocky areas, preferential flow parameters including macropore flow and lateral flow should be considered when studying soil water and groundwater (Jiang et al., 2017).

In Dinghushan area, soil conditions involved in plant roots and stones potentially contributed to the occurrence and development of preferential flow, including macropore flow and lateral flow. Besides the pore channels from rocks, the positive effects from plant root systems on water flow have also been extensively demonstrated in previous studies (Yue et al., 2021; Jiang et al., 2020). In this study, dyeing area increased with the increasing root biomass. Thus, the presence of roots promoted the active water flow. It has been confirmed in previous study that preferential flow guided by root systems affected groundwater recharge (Zhao and Wang, 2021; Li et al., 2017). However, a study indicated that deep roots in unsaturated zones reduced groundwater recharge by>50

% (compared with shallow roots) due to plant higher water consumption. Although the root systems can preferentially guide surface water to the deep soil, the recharge amount of groundwater by rainfall will still be greatly reduced or eliminated (Li et al., 2018). Therefore, the interaction mechanisms between soil conditions (e.g., pore connectivity) and water flow paths need further consideration for providing more hydrological preconditions of plant water use and groundwater along the vegetation succession sequences (Dorau et al., 2022; Budhathoki et al., 2022).

5. Conclusion

The current study mainly investigated the characteristic of soil physical properties and hydraulic properties of the different succession stages of subtropical forests, pine forest (PF), mixed pine and broadleaf forest (MF) and monsoon evergreen broadleaf forest (BF). Comparing the soil physical properties of the three forest types, both BF and MF have a lower bulk density and higher porosity than PF. The soils of BF and MF show higher hydraulic conductivity and water holding capacity than PF, as a result of soil porosity. Consequently, soil physical properties were improved along forest succession sequences PF → MF → BF, thereby soil infiltrability and water holding capacity were also promoted.

The pattern of forest soil water flow was precisely revealed by using the dyeing tracer method. Results indicated that preferential flow, including vertical and lateral flow, exists and presents spatial variability in the three forest types. Soil pores created water flow paths, especially the macropore channels from root systems and stones made preferential flow more active. Correlation analysis showed that the dense soil (bulk density) had lower water conductivity, which were not conducive to water exchange; while soil-rock interfaces, root systems and other pore channels can significantly promote water flow patterns. Soil water flow patterns varied greatly in different regions; preferential flow degree was verified to be not ordered by forest succession stages. Although some soil properties can be improved along forest succession sequences, soil water flow patterns were potentially uncontrollable due to the complex conditions of the soil. Therefore, for forest water resource conservation, in the active preferential flow areas, more attention should be paid to changes in the quantity and quality of deeper soil water and groundwater; while in the slow infiltration and flow areas, some measures should be taken for surface runoff and soil erosion in the forest land.

Declaration of Competing Interest

The authors declare that they have no known competing financial interests or personal relationships that could have appeared to influence the work reported in this paper.

Data availability

No data was used for the research described in the article.

Acknowledgements

The authors deeply appreciate editors and three anonymous reviewers for their constructive comments. This study was jointly funded by The Key Research and Development Program of Guangdong Province (Grant No. 2020B1111530004), the National Natural Science Foundation of China (Grant Nos. 41977287, 41991285 and 32101342) and the China Postdoctoral Science Foundation (Grant Nos. 2021 M703259, 2021 M703260, 2021 M693220).

Appendix A. Supplementary material

Supplementary data to this article can be found online at https://doi.org/10.1016/j.catena.2022.106748.

References

Alaoui, A., Helbling, A., 2006. Evaluation of soil compaction using hydrodynamic water content variation: comparison between compacted and non-compacted soil. Geoderma 134 (1–2), 97–108.
Allaire, S.E., Roulier, S., et al., 2009. Quantifying preferential flow in soils: a review of different techniques. J. Hydrol. 378, 179–204.
Ameli, A.A., Amvrosiadi, N., et al., 2016. Hillslope permeability architecture controls on subsurface transit time distribution and flow paths. J. Hydrol. 543 (Part A), 17–30.
Anderson, A.E., Weiler, M., et al., 2009. Subsurface flow velocities in a hillslope with lateral preferential flow. Water Resour. Res. 45, w11407.
Bargués Tobella, A., Reese, H., et al., 2014. The effect of trees on preferential flow and soil infiltrability in an agroforestry parkland in semiarid Burkina Faso. Water Resour. Res. 50 (4), 3342–3354.
Bens, O., Wahl, N.A., et al., 2007. Water infiltration and hydraulic conductivity in sandy cambisols: impacts of forest transformation on soil hydrological properties. Eur. J. For. Res. 126, 101–109.
Beven, K., Germann, P., 1982. Macropores and water flow in soils. Water Resour. Res. 18, 1311–1325.
Bisantino, T., Bingner, R., et al., 2015. Estimation of runoff, peak discharge and sediment load at the event scale in a medium-size Mediterranean watershed using the Annagnps Model. Land Degrad. Dev. 26, 340–355.
Bodhinayake, W., Si, B.C., et al., 2004. Determination of hydraulic properties in sloping landscapes from tension and double-ring infiltrometers. Vadose Zone J. 3 (3), 964–970.
Budhathoki, S., Lamba, J., et al., 2022. Using X-ray computed tomography to quantify variability in soil macropore characteristics in pastures. Soil Tillage Res. 215, 105194.
Buol, S.W., Southard, R.J., et al., 2003. Soil genesis and classification. Iowa State Press.
Chae, H.M., Choi, S.H., et al., 2019. Effect of litter quality on needle decomposition for four pine species in Korea. Forests 10 (5), 371.
Crockford, R.H., Richardson, D.P., 2000. Partitioning of rainfall into throughfall, stemflow and interception: effect of forest type, ground cover and climate. Hydrol. Process. 14 (1617), 2903–2920.
Di Prima, S., Bagarello, V., et al., 2017. Impacts of thinning of a Mediterranean oak forest on soil properties influencing water infiltration. J. Hydrol. Hydromech. 276–286.
Di Prima, S., Marrosu, R., et al., 2018. In situ characterization of preferential flow by combining plot- and point-scale infiltration experiments on a hillslope. J. Hydrol. 563, 633–642.
Doerr, S.H., Shakesby, R.A., et al., 2000. Soil water repellency: its causes, characteristics and hydro-geomorphological significance. Earth-Sci. Rev. 51, 33–65.
Dorau, K., Uteau, D., et al., 2022. Soil aeration and redox potential as function of pore connectivity unravelled by x-ray microtomography imaging. Eur. J. Soil Sci. 73, e13165.
Flury, M., Fluhler, H., et al., 1994. Susceptibility of soils to preferential flow of water: a field study. Water Resour. Res. 30 (7), 1945–1954.
Fuhrmann, I., Maarastawi, S., et al., 2019. Preferential flow pathways in paddy rice soils as hot spots for nutrient cycling. Geoderma 337, 594–606.
Gardner, W.R., Hillel, D., et al., 1970. Post-irrigation movement of soil water: 1. redistribution. Water Resour. Res. 6, 851–861.
He, Z.B., Zhao, M.M., et al., 2019. Temporal stability of soil water storage in multiple soil layers in high-elevation forests. J. Hydrol. 569, 532–545.
Heathman, G.C., Cosh, M.H., et al., 2012. Multi-scale temporal stability analysis of surface and subsurface soil moisture within the Upper Cedar Creek Watershed, Indiana. Catena 95, 91–103.
Hlaváčiková, H., Holko, L., et al., 2019. Estimation of macropore flow characteristics in stony soils of a small mountain catchment. J. Hydrol. 574, 1176–1187.
Hua, F.Y., Bruijnzeel, L.A., et al., 2022. The biodiversity and ecosystem service contributions and trade-offs of forest restoration approaches. Science 376 (6595), 839–844.
Jačka, L., Walmsley, A., et al., 2021. Effects of different tree species on infiltration and preferential flow in soils developing at a clayey spoil heap. Geoderma 115372.
Jiang, X.J., Li, X.G., 2015. Assessing the effects of plastic film fully mulched ridge-furrow on rainwater distribution in soil using dye tracer and simulated rainfall. Soil Tillage Res. 15267–15273.
Jiang, X.J., Liu, S., et al., 2017. Effects of different management practices on vertical soil water flow patterns in the Loess Plateau. Soil Tillage Res. 166, 33–42.
Jiang, X.J., Zakari, S., et al., 2020. Can complementary preferential flow and non-preferential flow domains contribute to soil water supply for rubber plantation? For. Ecol. Manag. 461, 117948.
Jørgensen, P.R., Hoffmann, M., et al., 2002. Preferential flow and pesticide transport in a clay-rich till: field, laboratory, and modeling analysis. Water Resour. Res. 38 (11), 28–1–28-15.
King, P.M., 1981. Comparison of methods for measuring severity of water repellence of sandy soils and assessment of sandy soils and assessment of some factors that affect its measurement. Australian J. Soil Res. 19, 275–285.
Kottek, M., Grieser, J., et al., 2006. World map of the Köppen-Geiger climate classification updated.
Kuchment, L.S., 2022. The Effects of Forest on Annual Water Yield of River Watershed. Water Resour. 49, 38–45.
Kurzweil, J.R., Metlen, K., et al., 2021. Surface water runoff response to forest management: Low-intensity forest restoration does not increase surface water yields. For. Ecol. Manag. 496, 119387.
Li, Z., Chen, X., et al., 2017. Determination of groundwater recharge mechanism in the deep loessial unsaturated zone by environmental tracers. Sci. Total Environ. 586, 827–835.

Li, H., Si, B.C., et al., 2018. Rooting depth controls potential groundwater recharge on hillslopes. J. Hydrol. 564, 164–174.
Liu, Y., Havrilla, C.A., et al., 2021. Litter crusts enhance soil nutrients through bacteria rather than fungi in sandy ecosystems. Catena 204, 105413.
Liu, P.L., Liu, X.D., et al., 2020. Influence of Vegetation Restoration on Soil Hydraulic Properties in South China. Forests 11 (10), 1–15.
Liu, X.D., Qiao, Y.N., et al., 2013. Water-holding characteristics of litters in three forests at different successional stages in Dinghushan. Scientia Silvae Sinicae 49 (09), 8–15. In Chinese.
Ludwig, J.A., Wilcox, B.P., et al., 2005. Vegetation patches and runoff-erosion as interacting ecohydrological processes in semiarid landscapes. Ecology 86, 288–297.
Mei, X.M., Zhu, Q.K., et al., 2018. Effect of stand origin and slope position on infiltration pattern and preferential flow on a loess hillslope. Land Degrad. Dev. 29, 1353–1365.
Neris, J., Tejedor, M., et al., 2013. Effect of forest floor characteristics on water repellency, infiltration, runoff and soil loss in andisols of tenerife (Canary Islands, Spain). Catena 108, 50–57.
Niemeyer, R.J., Fremier, A.K., et al., 2014. Woody vegetation increases saturated hydraulic conductivity in dry tropical Nicaragua. Vadose Zone J. 13 (1), 1–11.
Peng, X.D., Dai, Q.H., 2022. Drivers of soil erosion and subsurface loss by soil leakage during karst rocky desertification in SW China. Int. Soil Water Conserv. Res. 10 (2), 217–227.
Penna, D., Brocca, L., et al., 2013. Soil moisture temporal stability at different depths on two alpine hillslopes during wet and dry periods. J. Hydrol. 477, 55–71.
Piaszczyk, W., Lasota, J., et al., 2020. Effect of organic matter released from deadwood at different decomposition stages on physical properties of forest soil. Forests 11 (1), 24.
Reynolds, W.D., Elrick, D.E., 1990. Ponded infiltration from a single ring: I. analysis of steady flow. Soil Sci. Soc. Am. J. 54 (5), 1233.
Sheffer, E., Canham, C.D., et al., 2015. Countervailing effects on pine and oak leaf litter decomposition in human-altered Mediterranean ecosystems. Oecologia 177 (4), 1039–1051.
Sohrt, J., Ries, F., et al., 2014. Significance of preferential flow at the rock soil interface in a semi-arid karst environment. Catena 123, 1–10.
Song, L., Yang, B., et al., 2022. Spatial-temporal differentiations in water use of coexisting trees from a subtropical evergreen broadleaved forest in Southwest China. Agric. For. Meteorol. 316, 108862.
Soracco, C.G., Villarreal, R., et al., 2019. Hydraulic conductivity and pore connectivity. effects of conventional and no-till systems determined using a simple laboratory device. Geoderma 337, 1236–1244.
Šurda, P., Lichner, Ľ., et al., 2015. Effects of vegetation at different succession stages on soil properties and water flow in sandy soil. Biologia. 70 (11), 1474–1479.
van Schaik, N., 2009. Spatial variability of infiltration patterns related to site characteristics in a semi-arid watershed. Catena 78 (1), 36–47.
Wang, Z.H., Hou, Y., et al., 2012. Effects of plant species diversity on soil conservation and stability in the secondary succession phases of a semi-humid evergreen broadleaf forest in China. J. Soil Water Conserv. 67, 311–320.
Watanabe, T., Fukuzawa, K., et al., 2013. Temporal changes in litterfall, litter decomposition and their chemical composition in Sasa dwarf bamboo in a natural forest ecosystem of northern Japan. J. For. Res. 18 (2), 129–138.
Wine, M.L., Ochsner, T.E., et al., 2012. Effects of eastern redcedar encroachment on soil hydraulic properties along Oklahoma's grassland-forest ecotone. Hydrol. Process. 26 (11), 1720–1728.
WRB, 2015. World Reference Base for Soil Resources 2014. Update 2015. World Soil Resources Reports No. 106. Food and Agriculture Organization of the United Nations, Rome, 192 p.
Yan, J.H., Zhou, G.Y., et al., 2007. Changes of soil water, organic matter, and exchangeable cations along a forest successional gradient in Southern China. Pedosphere 17, 397–405.
Yu, X.N., Huang, Y.M., et al., 2018. Effects of rainfall and vegetation to soil water input and output processes in the Mu Us Sandy Land, northwest China. Catena 161, 96–103.
Yue, L., Wang, Y., et al., 2021. Impacts of soil compaction and historical soybean variety growth on soil macropore structure. Soil Tillage Res. 214 (1–2), 105166.
Zhang, Y.W., Deng, L., et al., 2016b. Interaction of soil water storage dynamics and long-term natural vegetation succession on the loess plateau, China. Catena 137, 52–60.
Zhang, Y., Zhang, M., et al., 2016a. Rock fragments and soil hydrological processes: significance and progress. Catena 147, 153–166.
Zhao, G.Q., Gao, Y., et al., 2019. Isotopically-tracked hydrological changes in carbon cycling and its sources in a Chinese subtropical forested watershed. J. Hydrol. 575, 1041–1051.
Zhao, Y., Wang, L., 2021. Determination of groundwater recharge processes and evaluation of the 'two water worlds' hypothesis at a check dam on the Loess Plateau. J. Hydrol. 595, 125989.
Zhao, S., Zhao, Y., et al., 2010. Quantitative analysis of soil pores under natural vegetation successions on the Loess Plateau. Sci. China Earth Sci. 53, 617–625.
Zhou, G.Y., Wei, X.H., et al., 2011. Quantifying the hydrological responses to climate change in an intact forested small watershed in Southern China. Glob. Chang. Biol. 17 (12), 3736–3746.
Zhu, X.A., Chen, C.F., et al., 2019. Can intercrops improve soil water infiltrability and preferential flow in rubber-based agroforestry system? Soil Tillage Res. 191, 327–339.
Zhu, X.A., Zhang, W.J., et al., 2021. Conversion of primary tropical rainforest into rubber plantation degrades the hydrological functions of forest litter: insights from experimental study. Catena 200, 105172.